Int. J. Heat Mass Transfer. Vol. 28, No. 5, pp. 949–957, 1985
Printed in Great Britain
0017-9310/85 $3.00 + 0.00

Steady-state characteristics and stability thresholds of a closed two-phase thermosyphon

FLAVIO DOBRAN
Stevens Institute of Technology, Hoboken, NJ 07030, U.S.A.

(*Received* 12 *June* 1984 *and in final form* 13 *November* 1984)

Abstract—An analytical investigation is presented for the purpose of determining the steady-state characteristics and stability thresholds of a closed two-phase thermosyphon. The analytical model is based on a lumped parameter description of the system that includes the thermohydraulics of vapor core, liquid film, and liquid pool of the evaporator. The steady-state solutions and the linear stability analysis of the governing equations revealed the existence of two operating limits: one associated with flooding and the other with drying of the liquid in the evaporator. A parametric study was also performed to determine the effects of heat pipe geometry, liquid filling, and fluid characteristics on the operating limits. The comparison of the predicted limiting heat fluxes of flooding and dry-out with the experimental data was also performed.

1. INTRODUCTION

A CLOSED two-phase thermosyphon is a gravity-assisted wickless heat pipe with liquid reservoir at the bottom. The addition of heat to the liquid causes the liquid to evaporate; the vapor rises to the top of the tube where it is condensed and the condensate returns to the evaporator section by gravity as a falling liquid film. Experimental studies [1–11] of closed two-phase thermosyphons show the existence of several operating limits that depend on the heat addition to the evaporator, geometry of the thermosyphon (tube diameter and length, length of the evaporator and condenser sections), liquid filling and fluid characteristics. These operating limits are identified in the literature as the dry-out limit, burn-out or critical heat flux limit, flooding limit, and the oscillation limit.

The *dry-out limit* can occur under the following conditions: (1) when the amount of working fluid is a minimum for the thermosyphon to have a continuous circulation of vapor and condensate at a given heat flux; and (2) when some portion of the liquid film region ceases to be cooled effectively. In the former case, when the working fluid is less than the required minimum, the liquid pool dries out resulting in the wall temperature excursion in the evaporator. The length of the dried surface in the evaporator depends on the heat input, liquid filling, working fluid, and operating system pressure but, unfortunately, not much is known about the detailed relationship between the variables which give rise to such a limiting operation. At high heat fluxes it is possible to reach the dry-out limit in the liquid film above the liquid pool level. This can occur due to the reinforcing effects of the high evaporation rate and interfacial shear whereby they prevent the downflow of liquid. The result is a local dry-out of the surface of thermosyphon leading to wall temperature excursion.

At high liquid fillings when the heat input is only to the liquid pool the thermosyphon operation can be limited by the *boiling or critical heat flux limit*. This limit is similar to the critical heat flux condition in pool boiling and it also leads to a temperature excursion of the tube surface [7, 11].

With large liquid fillings in long thermosyphons and at large axial and small radial heat fluxes, it is possible to establish another operating limit, the so-called *entrainment or flooding limit*. This limit occurs due to the instability of the liquid film generated by the high value of the interfacial shear which gives rise due to the high vapor velocity induced by high heat fluxes. The high vapor shear gives rise to the entrainment of liquid from the film into the vapor core and, consequently, to a flooding condition. This leaves the liquid film thin and the evaporator surface can become dry resulting again in wall temperature excursion or limiting system operation. By increasing the heat flux above the flooding limit, it is possible to achieve the liquid film flow reversal leading to: (1) the accumulation of liquid in the condenser; (2) falling of the accumulated liquid due to gravity to the evaporator; (3) establishment of a film flow situation again; and (4) the occurrence of flooding and film flow reversal whereby the cycle repeats itself [11]. Since this process has associated with it large pressure and temperature oscillations of the fluid (on the order of 300°C), the heat flux condition leading to this system operation is referred to as the *oscillation limit* [11].

From the above, it is clear that the operating limits of a closed two-phase thermosyphon depend on many parameters. These are the input heat flux rate to the evaporator and its distribution, geometry of the thermosyphon, working fluid, liquid filling and operating pressure or temperature of the fluid. While it is possible to model analytically various limiting situations of a closed thermosyphon separately (dryout, critical heat flux, and flooding), it has not yet

NOMENCLATURE

Ca	capillary number, $\mu_L^2/(\sigma\rho_L D)$
C_L	specific heat of liquid
D	pipe diameter
fi	interfacial friction coefficient
fw	wall friction coefficient
g	gravitational constant
h; h^*	liquid filling height in the evaporator; $Q_L/(\pi R^3)$
h_{LG}	enthalpy of evaporation
l; l^*	thermosyphon pipe length; l/R
N_L	two-phase Grashof number, $(gD^3\rho_L^2/\mu_L^2)^{1/2}$
Q_i; Q_i^*	heat input to the evaporator; $Q_i/(8\mu_L R h_{LG})$
Q_L	liquid filling
R	pipe radius
Re	Reynolds number
t; t^*	time; $tQ_i/(\rho_L h_{LG} R^3)$
T	temperature
u_1	defined by equation (20)
u_2	defined by equation (21)
x_1^*	nondimensional liquid film length, $\tilde{z}/R$
x_2^*	nondimensional film cross-sectional area, $\tilde{\delta}\tilde{z}/R^2$
x_3^*	nondimensional film temperature, $(\tilde{T}_L - T_s)/T_s$
x_4^*	nondimensional film velocity, $\frac{d\tilde{z}}{dt}\rho_L R^2 h_{LG}/Q_i$
$\tilde{z}$	film length defined in Fig. 1b.

Greek symbols

$\Gamma_{c\tilde{z}}$; $\Gamma_{c\tilde{z}}^*$	condensation mass flow-rate per unit pipe periphery; $\Gamma_{c\tilde{z}} h_{LG} R/Q_i$
Γ_L; Γ_L^*	liquid film mass flow-rate at $\tilde{z}$ per unit pipe periphery; $\Gamma_L h_{LG} R/Q_i$
$\tilde{\delta}$	average film thickness
μ; μ^*	viscosity; μ_G/μ_L
ρ; ρ^*	density; ρ_G/ρ_L
σ	surface tension
τ	shear stress.

Subscripts

G	pertains to the vapor
i	pertains to the interface
l	laminar
L	pertains to the liquid
s	saturation valve
w	wall.

proved feasible to predict quantitatively within one model the occurrence of more than one limiting condition as a function of the arbitrary parameters of the system. Although a considerable data base already exists on the two-phase thermosyphons, it should be noted that some of these data are incomplete and cannot be utilized for the verification of more complex models, and much more data are clearly needed not only to delineate stable and unstable regions of operation as a function of the parameters of the system enumerated above, but also to guide the analysts in the construction of more sophisticated physical models for the prediction of steady-state and transient system behaviors.

The objective in this paper is to construct a model of the hydrodynamic and heat transfer processes of a closed two-phase thermosyphon in order to determine the steady-state and stability thresholds as a function of independent system parameters. For this purpose, a simple lumped parameter description of the system is performed and the resulting mathematical model is examined for stability limits. It is found that the model yields two types of heat flux limits: one that is associated with the dry-out of the liquid pool and the other which is associated with the instability of the liquid film or flooding.

2. ANALYSIS

A typical operating condition of a closed two-phase thermosyphon is illustrated in Fig. 1(a). The thermosy-

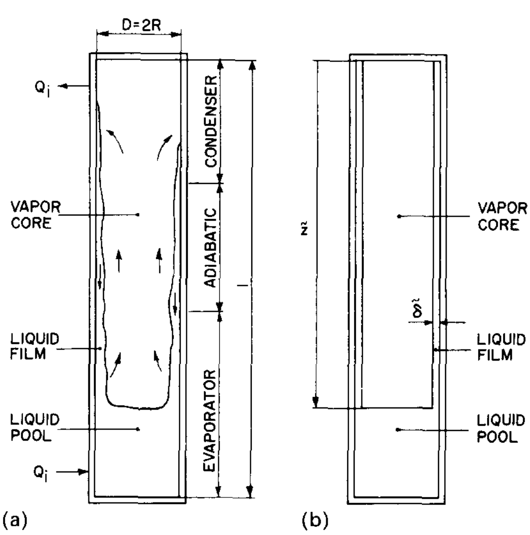

FIG. 1. (a) Actual two-phase flow in a thermosyphon; (b) idealized flow in a thermosyphon.

phon consists of an internal pipe diameter $D = 2R$, length l, and of the evaporator and condenser sections at the pipe bottom and top, respectively. Due to the heat addition in the evaporator, the liquid evaporates from the liquid pool and film regions; the vapor rises along the central core region of the pipe and is condensed on the wall in the condenser portion. The liquid then drains by gravity along the pipe surface to the liquid pool. In reality, the liquid film thickness is not uniform (due to the evaporation and condensation) and usually not smooth, and may be covered by a complex system of waves. However, for the purpose of constructing a model, it will be assumed that the film can be represented by an average film thickness $\tilde{\delta}$ as illustrated in Fig. 1(b). The vertical distance from the top of the pipe to the liquid pool surface will be denoted by $\tilde{z}$, the average film temperature by $\tilde{T}_L$, and the liquid pool and vapor core are assumed to be saturated at T_s. The film is also assumed to be thin, $\delta \ll R$, and the operation of the thermosyphon away from the thermodynamic critical point, $\rho_G/\rho_L \ll 1$.

2.1. *Lumped parameter analysis*

Denoting by $\Gamma_{c\tilde{z}}$ the mass flow-rate of vapor condensation per unit tube periphery ($2\pi R$) onto the liquid film and by Γ_L the mass flow-rate of liquid per unit tube periphery flowing (at $\tilde{z}$) into the liquid pool, we have from the control volume mass and energy balances on the liquid film and pool:

$$\frac{d\tilde{\delta}\tilde{z}}{dt} = \frac{\Gamma_{c\tilde{z}} - \Gamma_L}{\rho_L} \tag{1}$$

$$\tilde{\delta}\tilde{z}\frac{d\tilde{T}_L}{dt} = \frac{\Gamma_{c\tilde{z}}}{\rho_L C_L}[h_{LG} - C_L(\tilde{T}_L - T_s)] - \frac{Q_i}{2\pi R \rho_L C_L} \tag{2}$$

$$\Gamma_L = \frac{Q_i - \rho_L \pi R^2 h_{LG}\dfrac{d\tilde{z}}{dt}}{2\pi R[h_{LG} - C_L(\tilde{T}_L - T_s)]} \tag{3}$$

where Q_i is the heat supplied to the evaporator. Similarly, a control volume momentum balance on the liquid film and vapor core yields:

$$\begin{aligned} 2\rho_L\tilde{\delta}\tilde{z}\frac{d^2\tilde{z}}{dt^2} = & -\tilde{z}\frac{d\Gamma_L}{dt} - \frac{d\tilde{z}}{dt}\left[\Gamma_L\left(1 - 4\frac{\rho_L}{\rho_G}\frac{\tilde{\delta}}{R}\right)\right. \\ & + 2\frac{\rho_G}{\rho_L}\frac{\tilde{\delta}}{R}\Gamma_{c\tilde{z}} + \left(\frac{fw}{fw_l}\right)2\mu_L\frac{\tilde{z}}{\tilde{\delta}} \\ & \left. + \left(\frac{fi}{fi_l}\right)4\mu_G\frac{\tilde{z}}{R}\frac{\rho_L}{\rho_G}\right] + \frac{\Gamma_L}{\rho_L\tilde{\delta}}\left[\Gamma_{c\tilde{z}} - \Gamma_L\right. \\ & \times\left(1 - 4\frac{\rho_L}{\rho_G}\frac{\tilde{\delta}^2}{R^2}\right) - \left(\frac{fw}{fw_l}\right) \\ & \left. \times 2\mu_L\frac{\tilde{z}}{\tilde{\delta}} - \left(\frac{fi}{fi_l}\right)4\mu_G\frac{\tilde{z}}{R}\left(1 + \frac{\rho_L}{\rho_G}\frac{2\tilde{\delta}}{R}\right)\right] \\ & + g\tilde{\delta}\tilde{z}\rho_L + \frac{\rho_L}{\rho_G}\rho_L\tilde{\delta}\left(\frac{d\tilde{z}}{dt}\right)^2 \end{aligned} \tag{4}$$

where fw and fi are the wall and interfacial friction coefficients, respectively, and fw_l and fi_l are their corresponding laminar values. The wall and interfacial shear stresses used in the momentum equation (4) are of the form:

$$\tau_w = \left(\frac{fw}{fw_l}\right)\frac{2\mu_L}{\tilde{\delta}}\left[\frac{\Gamma_L}{\rho_L\tilde{\delta}} + \frac{d\tilde{z}}{dt}\right] \tag{5}$$

$$\tau_i = \left(\frac{fi}{fi_l}\right)\frac{4\mu_G}{R}\left[\frac{\Gamma_L}{\rho_L\tilde{\delta}}\left(1 + \frac{\rho_L}{\rho_G}\frac{2\tilde{\delta}}{R}\right) + \frac{\rho_L}{\rho_G}\frac{d\tilde{z}}{dt}\right]. \tag{6}$$

There is one additional equation expressing the conservation of mass of the total fluid in the thermosyphon that has to be used, i.e.

$$\frac{Q_L}{\pi R^2 \tilde{z}} = \frac{l}{\tilde{z}} - \left(1 - \frac{\tilde{\delta}}{R}\right)^2\left(1 - \frac{\rho_G}{\rho_L}\right) \simeq \frac{l}{\tilde{z}} - \left(1 - \frac{\tilde{\delta}}{R}\right)^2 \tag{7}$$

Q_L in this equation is the (volumetric) liquid filling and it is an independent parameter of the system.

The system of nonlinear equations (1)–(7) is sufficiently complex and its solution will not be investigated in this paper. Instead, only a special case corresponding to the saturated liquid film will be considered below.

Assuming that $\tilde{T}_L = T_s$ in the above equations and performing the nondimensionalization of these equations according to:

$$x_1^* = \frac{\tilde{z}}{R}, \quad x_2^* = \frac{\tilde{\delta}\tilde{z}}{R^2}, \quad x_4^* = \frac{R^2\rho_L h_{LG}}{Q_i}\frac{d\tilde{z}}{dt}, \quad t^* = \frac{tQ_i}{\rho_L h_{LG} R^3} \tag{8}$$

$$\Gamma_{c\tilde{z}}^* = \Gamma_{c\tilde{z}}\frac{h_{LG}R}{Q_i}, \quad \Gamma_L^* = \Gamma_L\frac{h_{LG}R}{Q_i}, \quad Q_i^* = \frac{Q_i}{8\mu_L R h_{LG}}, \tag{9}$$

$$N_L^2 = \frac{gD^3\rho_L^2}{\mu_L^2}, \quad h^* = \frac{Q_L}{\pi R^3}, \quad l^* = \frac{l}{R}, \quad \mu^* = \frac{\mu_G}{\mu_L}, \quad \rho^* = \frac{\rho_G}{\rho_L} \tag{10}$$

results in the following system of equations:

$$\Gamma_{c\tilde{z}}^* = \frac{1}{2\pi} \tag{11}$$

$$\Gamma_L^* = \frac{1}{2\pi} - \frac{1}{2}x_4^* = \Gamma_{c\tilde{z}} - \frac{1}{2}x_4^* \tag{12}$$

$$\frac{x_2^*}{x_1^*} = \frac{1}{2}\left(1 - \frac{l^* - h^*}{x_1^*}\right) \tag{13}$$

$$\frac{dx_2^*}{dt^*} = \frac{1}{2}x_4^* \tag{14}$$

$$\frac{dx_4^*}{dt^*} = \frac{1}{[2x_2^* - (l^* - h^*)]}\left\{-2x_4^*\left[\Gamma_L^*\left(1 - \frac{4}{\rho^*}\frac{x_2^*}{x_1^*}\right) + \frac{\rho^*}{\pi}\frac{x_2^*}{x_1^*} + \frac{1}{Q_i^*}\left(\frac{fw}{fw_l}\right)\frac{1}{4}\frac{(x_1^*)^2}{x_2^*} + \frac{\mu^*}{Q_i^*}\left(\frac{fi}{fi_l}\right)\frac{x_1^*}{2\rho^*}\right]\right.$$
$$+ \frac{2\Gamma_L^* x_1^*}{x_2^*}\left[\frac{x_4^*}{2} + \Gamma_L^*\frac{4}{\rho^*}\left(\frac{x_2^*}{x_1^*}\right)^2 - \frac{1}{Q_i^*}\left(\frac{fw}{fw_l}\right) \times \frac{1}{4}\frac{(x_1^*)^2}{x_2^*} - \frac{\mu^*}{2Q_i^*}\left(\frac{fi}{fi_l}\right)x_1^*\left(1 + \frac{2x_2^*}{\rho^* x_1^*}\right)\right]$$
$$\left. + \frac{2x_2^*(x_4^*)^2}{\rho^* x_1^*} + N_L^2\frac{x_2^*}{256(Q_i^*)^2}\right\}. \quad (15)$$

Equations (11)–(15) have to be closed by specifying the constitutive equations for (fw/fw_l) and (fi/fi_l) for turbulent flow in the liquid film and vapor core, and to determine whether the flow is laminar or turbulent a decision can be made based on the Reynolds numbers for the liquid film, Re_L, and vapor core, Re_G, i.e. (ref. [12])

$$Re_L \equiv 32Q_i^*\left|\Gamma_L^* + \frac{x_2^*}{x_1^*}x_4^*\right| \begin{cases} < 1000 \text{ laminar flow} \\ \geqslant 1000 \text{ turbulent flow} \end{cases} \quad (16)$$

$$Re_G \equiv \frac{16}{\mu^*}Q_i^*\left|\Gamma_L^*\left(2 + \rho^*\frac{x_1^*}{x_2^*}\right) + x_4^*\right| \begin{cases} < 2300 \text{ laminar flow} \\ \geqslant 2300 \text{ turbulent flow.} \end{cases} \quad (17)$$

For thin and turbulent liquid films, it can be assumed [12] that the wall friction coefficient can be expressed by the Blausius formula,

$$\left(\frac{fw}{fw_l}\right)_{\text{turb.}} = \frac{0.079}{16}\left|32Q_i^*\left(\Gamma_L^* + \frac{x_2^*}{x_1^*}x_4^*\right)\right|^{0.75}, \quad (18)$$

whereas to model the interfacial friction coefficient, it is necessary to take into consideration the countercurrent flow of liquid and vapor. For this purpose, Bharathan *et al.*'s [13] correlation for fi will be utilized which was determined on the basis of air-water flooding data for wide range of pipe diameters and liquid and gas flowrates. Thus

$$\frac{fi}{fi_l} = \frac{Q_i^*}{\mu^*}\left[0.005 + u_1\left(\frac{N_L Ca^{1/2}}{2}\frac{x_2^*}{x_1^*}\right)^{u_2}\right] \times \left[\Gamma_L^*\left(2 + \rho^*\frac{x_1^*}{x_2^*}\right) + x_4^*\right] \quad (19)$$

where

$$u_1 = 0.2754 \times 10^{9.07/(N_L Ca^{1/2})} \quad (20)$$

$$u_2 = 1.63 + 4.74/(N_L Ca^{1/2}), \quad (21)$$

and

$$Ca \equiv \frac{\mu_L^2}{\sigma \rho_L D} \quad (22)$$

is the capillary number which represents the ratio of viscous to surface tension forces. Note that the group of parameters $N_L Ca^{1/2}$ is referred in the literature as the Bond number [13].

Equations (11)–(22) form a closed system of equations for the investigation of transient response of the thermosyphon with the arbitrary system parameters as follows:

Q_i^* heat supply parameter
N_L two-phase Grashof number
Ca capillary number
ρ^* density ratio (or buoyancy number, $Bo = 1 - \rho^*$)
μ^* viscosity ratio parameter
h^* liquid filling charge parameter
l^* tube length parameter. (23)

Steady-state analysis. A particularly simple solution can be obtained for the steady state where $dx_2^*/dt^* = 0$, $x_4^* = 0$, $dx_4^*/dt^* = 0$, $x_1^* = x_{10}^*$ and $x_2^* = x_{20}^*$. In this situation, from equation (12) $\Gamma_L^* = 1/2\pi$ and equation (15) is reduced to

$$Q_i^{*2}\left[\frac{2}{\pi\rho^*}\left(\frac{x_{20}^*}{x_{10}^*}\right)^2\right] - Q_i^*\left[\left(\frac{fw}{fw_l}\right)\frac{x_{10}^*}{4}\frac{x_{10}^*}{x_{20}^*} + \left(\frac{fi}{fi_l}\right)\frac{\mu^*}{2}x_{10}^*\left(1 + \frac{2}{\rho^*}\frac{x_{20}^*}{x_{10}^*}\right)\right] + N_L^2\frac{\pi}{256}x_{10}^*\left(\frac{x_{20}^*}{x_{10}^*}\right)^2 = 0. \quad (24)$$

From equation (13) we can solve for x_{10}^*

$$x_{10}^* = \frac{l^* - h^*}{1 - 2\dfrac{x_{20}^*}{x_{10}^*}} \quad (25)$$

and thus eliminate the dependence of equation (24) on the variable x_{10}^*. With this substitution, the physical ($Q_i^* \geqslant 0$) solution space of equations (18), (19) and (24) appears as illustrated in Fig. 2 in a plot of the heat input parameter Q_i^* vs the steady-state film thickness $x_{20}^*/x_{10}^* = \bar{\delta}/R$ as a function of the two-phase Grashof number N_L and liquid filling charge parameter h^*/l^* for fixed values of Ca, ρ^*, μ^* and l^*. As shown in Fig. 2, when $Q_i^* = 0$ then $x_{20}^*/x_{10}^* = 0$ as it is physically required, but an increase in the heat flux causes the film thickness also to increase. However, for a given value of N_L, Ca, ρ^*, μ^*, l^* and sufficiently large h^*/l^*, there is a maximum value of the heat flux which, as shown below, corresponds to the entrainment limiting operation of a thermosyphon. The film thickness can be increased until $x_1^* = l^*$ at which point the liquid pool becomes dry. This film thickness can be determined from equation (13), i.e.

$$\left(\frac{x_{20}^*}{x_{10}^*}\right)_{\max} = \frac{1}{2}\left[1 - \frac{l^* - h^*}{l^*}\right] = \frac{1}{2}\frac{h^*}{l^*} \quad (26)$$

and, therefore, the limiting solution of equation (24) can be expressed in terms of h^*/l^* as shown in Fig. 2 with

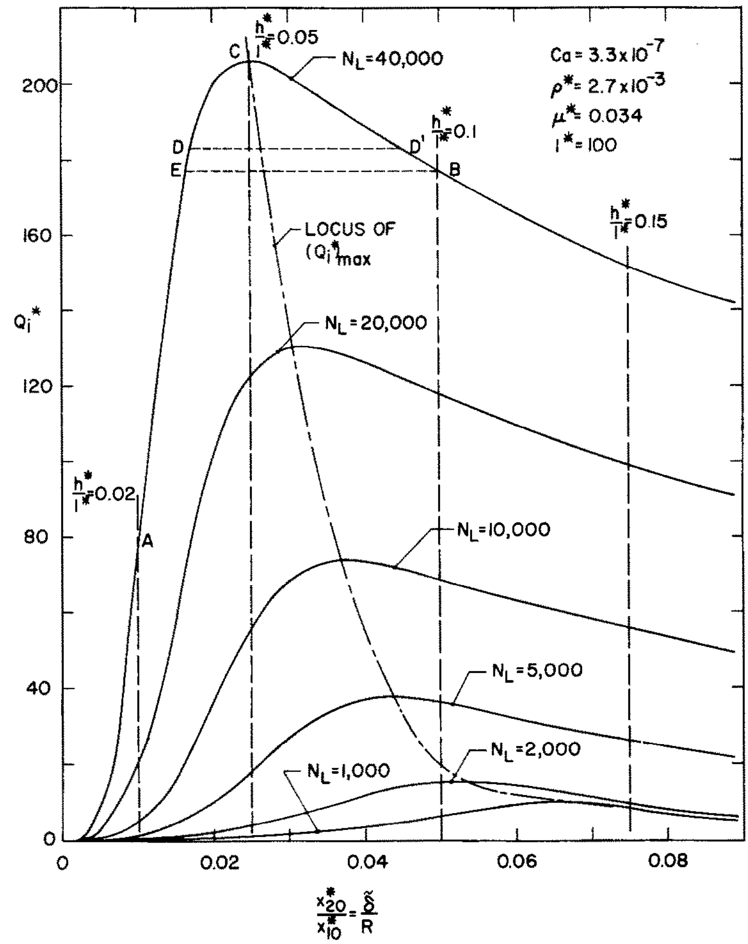

FIG. 2. Steady-state distribution of input heat flux to the evaporator with the film thickness.

vertical dotted lines. Notice that at low liquid fillings ($h^*/l^* \ll 1$), the dry-out of the liquid pool can occur before achieving the maximum heat flux condition (point A, for example, in Fig. 2 on the curve N_L = 40,000), whereas at large liquid fillings (point B), the steady-state solution predicts a maximum heat input to the evaporator that will sustain the steady state (at point C). As N_L decreases due to a decrease in the tube diameter, for example, $(Q_i^*)_{max}$ is reduced and shifted towards a larger film thickness. The effect of increasing the system pressure or increasing ρ^* is to increase the maximum heat flux with other parameters remaining the same and is not shown in Fig. 2. It is clear from Fig. 2 that an increase in Q_i^* above its maximum value $(Q_i^*)_{max}$ for fixed values of the remaining independent parameters cannot yield a steady-state solution since no film thickness exists which can maintain this new heat flux, and at this point the system operation may shift to a different state which may be either stable or unstable. With a given filling charge of $h^*/l^* = 0.1$ and $N_L = 40{,}000$ in Fig. 2, there are two different film thicknesses corresponding to the same heat flux; for example, $(Q_i^*)_D = (Q_i^*)_{D'}$. This means that fluctuations in the film thickness of sufficient magnitude may be able to produce the system operation between points D and D'. Figure 3 illustrates this in a plot of the nondimensional interfacial shear obtained from equation (6),

$$\tau_{i0}^* = \frac{\tau_{i0}}{\rho_L g 2R} = \frac{128(Q_i^*)^2}{\rho^* N_L^2} \times \left[0.005 + u_1\left(\frac{N_L^2 Ca^{1/2}}{2}\frac{x_{20}^*}{x_{10}^*}\right)^{u_2}\right] \times \left[\frac{1}{2\pi}\left(2+\rho^*\frac{x_{10}^*}{x_{20}^*}\right)\right]^2 \tag{27}$$

vs the heat input parameter Q_i^* as a function of N_L, Ca, ρ^*, μ^*, l^* and h^*/l^*.

To investigate analytically the dynamics of the liquid film and pool in a thermosyphon, it is necessary to investigate the solution of the nonlinear equations (11)–(19). In this paper, however, only the results from a linearized analysis will be discussed.

Linearized stability analysis. Equation (15) can be linearized about the equilibrium state x_{10}^*, x_{20}^* and

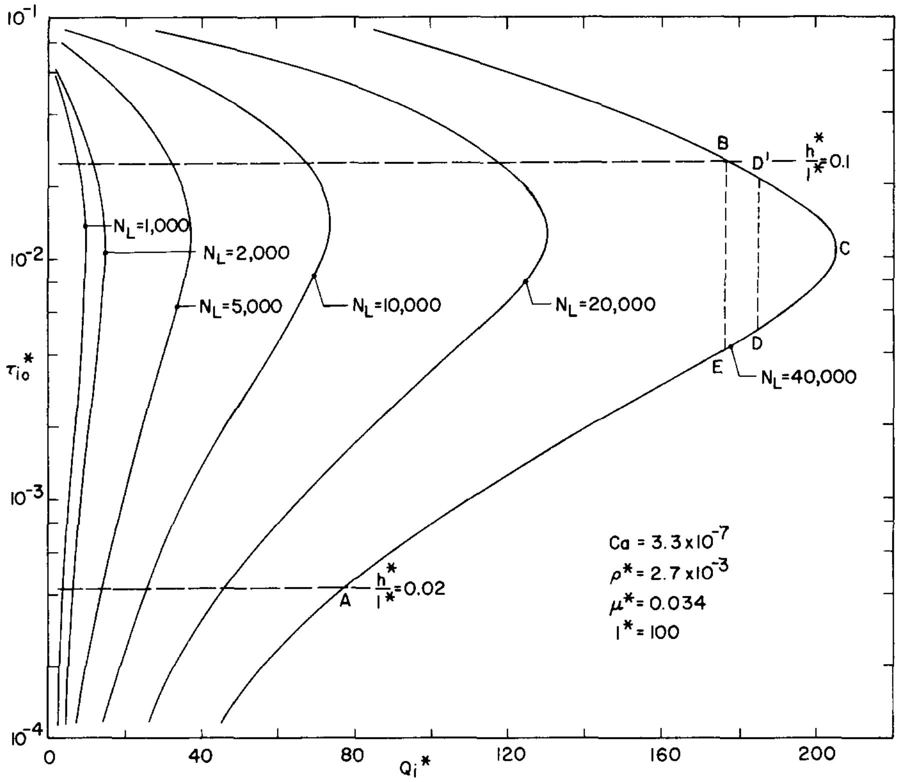

FIG. 3. Steady-state interfacial shear stress distribution.

$x_{40}^* = 0$, i.e.

$$\frac{dx_4^*}{dt^*} = f(x_1^*, x_4^*) = f(x_{10}^*, 0) + \left.\frac{\partial f}{\partial x_1^*}\right|_0 \times (x_1^* - x_{10}^*) + \left.\frac{\partial f}{\partial x_4^*}\right|_0 (x_4^* - 0) + F(x_1^*, x_4^*)$$

$$= A_{21}(x_1^* - x_{10}^*) + A_{22}(x_4^* - 0) + F(x_1^*, x_4^*) \quad (28)$$

where $f(x_{10}^*, 0) = 0$ represents the steady-state solution expressed by equation (24), whereas $A_{21} = \partial f/\partial x_1^*|_0$ and $A_{22} = \partial f/\partial x_4^*|_0$ are evaluated at the steady-state values of x_1^* and x_4^*. $F(x_1^*, x_4^*)$ denotes the nonlinear terms in the series expansion of equation (28). Since also from equation (8) we have that

$$\frac{dx_1^*}{dt^*} = x_4^*, \quad (29)$$

equations (28) and (29) can be written as follows:

$$\begin{pmatrix} \dfrac{dx_1^*}{dt^*} \\ \dfrac{dx_4^*}{dt^*} \end{pmatrix} = \begin{pmatrix} 0 & 1 \\ A_{21} & A_{22} \end{pmatrix} \begin{pmatrix} x_1^* - x_{10}^* \\ x_4^* - 0 \end{pmatrix} + \begin{pmatrix} 0 \\ F \end{pmatrix}. \quad (30)$$

The necessary and sufficient conditions for the above system of equations to yield stable steady-state solutions are that the eigenvalues of the characteristic equation, det $|A - \lambda I| = 0$, have negative real parts. The analysis shows that, as the heat flux to the evaporator is increased, there is a progressive loss of stability of the system (the eigenvalues of equation (30) became less negative) and that the steady-state solution becomes unstable when the liquid pool dries out, that is when $x_{10}^* = l^*$ and $Q_i^* \leqslant (Q_i^*)_{max}$. The steady state is also unstable for large liquid fillings when $Q_i^* = (Q_i^*)_{max}$, since at this point one of the eigenvalues has a turning point from the negative to the positive value. The instability of the system at large liquid fillings and at the maximum values of heat fluxes shown in Fig. 2 is also consistent with the experimental observations and, as discussed below, it can be physically associated with the entrainment or flooding limiting operation of the thermosyphon.

3. DISCUSSION AND COMPARISON OF THE ANALYTICAL RESULTS WITH EXPERIMENTS

The analytical results of the limiting input heat fluxes to the evaporator, Q_i^*, presented and discussed in the previous section, are compared with the experimental data in this section. Much of the data in the literature pertaining to the limiting heat fluxes cannot be used for the comparison with the analytical results either because of the lack of complete parameter specification in the experiments as required by the model [equation

Table 1. Comparison between the experimental and predicted heat fluxes and their dependence on the system parameters

References	$l^* = \frac{l}{R}$	$h^* = \frac{Q_L}{\pi R^3}$	N_L	Ca	$\rho^* = \frac{\rho_G}{\rho_L}$	$\mu^* = \frac{\mu_G}{\mu_L}$	$(Q_i^*)_{exp}$ Nature of critical heat flux	Predicted heat flux limits $(Q_i^*)_{dry-out 1}$	Predicted heat flux limits $(Q_i^*)_{max}$	Predicted heat flux limits $(Q_i)_{dry-out 2}$
Fukano *et al.* [11] $2R = 0.953$–2.09 cm	87.5	14	23,300	3.3×10^{-7}	2.7×10^{-3}	0.034	69.5 Oscillation limit		146	107
$l = 91.44$ cm $Q_L = 10$–50 cm^3	191.5	29.5	5335	1.2×10^{-6}	1.2×10^{-3}	0.025	18.4 Film dryout limit		26.3	20
$P = 0.05$–0.4 MPa Methanol	191.5	73.6	9720	4.3×10^{-7}	5.6×10^{-3}	0.057	42.8 Evaporation critical heat flux		91.3	41
Nguyen-Chi and Groll [10]	294	45	14,740	1.94×10^{-7}	1.32×10^{-4}	0.023	27 Entrainment limit		31	18
$2R = 1.9$ cm $l = 250$ cm	294	45	12,608	2.6×10^{-7}	8.4×10^{-5}	0.0184	18.5 Entrainment limit		21.5	12.3
$Q_L = 86$–200 cm^3 $P = 0.004$–0.02 MPa	294	45	10,574	3.6×10^{-7}	5.15×10^{-5}	0.015	12.2 Entrainment limit		14.3	8.1
Water	294	45	8676	5.3×10^{-7}	3×10^{-5}	0.017	8.3 Entrainment limit		9.1	5.1
	294	104	14,740	1.94×10^{-7}	1.32×10^{-4}	0.023	26 Entrainment limit		31	10.3
	294	104	8676	5.3×10^{-7}	3.05×10^{-5}	0.017	6.5 Entrainment limit		9.1	3
Cohen and Bayley [1] $2R = 1.915$ cm	80	0.55	28,300	7.24×10^{-8}	6.23×10^{-4}	0.043	7.1 Evaporation critical heat flux	1.1		
$l = 76.2$ cm $Q_L = 1.5$–4 cm^3 $P = 0.1$ MPa	80	0.74	28,300	7.24×10^{-8}	6.23×10^{-4}	0.043	27 Evaporation critical heat flux	2.5		
Water	80	1.1	28,300	7.24×10^{-8}	6.23×10^{-4}	0.043	42 Evaporation critical heat flux	8.5		
	80	1.5	28,300	7.24×10^{-8}	6.23×10^{-4}	0.043	48 Evaporation critical heat flux	30		

(23)] or of the different thermosyphon geometries (open thermosyphon, annular thermosyphon, etc.) utilized in these investigations. Table 1 shows a summary of three such experimental investigations where a comparison with the present model is possible. Given in this table are the independent parameters of the system (l^*, h^*, N_L, Ca, ρ^* and μ^*) and the observed limiting heat fluxes and their nature, i.e. pertaining to the oscillation limit [11], liquid film dry-out limit [11], entrainment limit [10] and the critical heat flux limit [1]. The last three columns in Table 1 show the predicted limiting fluxes by utilizing the steady state solution [equation (24)]. $(Q_i^*)_{max}$ is the maximum input heat flux corresponding to the given parameters (see Fig. 2), $(Q_i^*)_{dry\text{-}out\,2}$ corresponds to the situation when the liquid filling is large and the evaporator dries out (point B, for example, in Fig. 2), and $(Q_i)_{dry\text{-}out\,1}$ corresponds to the dry-out of the evaporator at small liquid fillings (point A in Fig. 2).

The comparison between the predicted and experimental values of limiting heat fluxes in Table 1 indicates that the heat fluxes due to the entrainment or flooding can be associated with $(Q_i^*)_{max}$, while the oscillation and film dry-out limiting fluxes compare most favorably with $(Q_i^*)_{dry\text{-}out\,2}$. It should be stressed, however, that this comparison is not meaningful since $(Q_i^*)_{dry\text{-}out\,2}$ corresponds to the drying of the evaporator, while the experimental film dry-out heat flux is associated with drying of the film above the surface of the liquid pool.

The limiting heat fluxes corresponding to the critical heat fluxes in the evaporator occur at low as well as at high liquid fillings depending on the input heat flux distribution. Table 1 shows some data points associated with such limiting fluxes and the corresponding fluxes from the analysis. As seen in this table, the model fails to predict the evaporator critical heat fluxes at low liquid fillings, since no physics is built into the model to achieve this prediction.

Lee and Mital's [3] experimental data, although quite thorough, cannot be utilized for comparison with this analysis because of their definition of the limiting heat flux which corresponds to a flux above which the operating pressure inside the thermosyphon tube cannot be maintained. Their definition of limiting heat fluxes leads in general to lower critical fluxes than those discussed above. Bezrodnyi and Volkov's [9] experimental data pertain to a closed thermosyphon connected to a large reservoir at the bottom filled with liquid. They identified three distinct limiting heat fluxes: (1) those associated with flooding; (2) those associated with the liquid film hanging; and (3) those associated with the liquid film inversion. Their data are expressed in terms of three different correlations reflecting the three crisis phenomena above whose direct comparison with the analysis presented in the paper is not straightforward. These experiments demonstrate, nevertheless, that the limiting heat fluxes associated with liquid film hanging and film inversion are greater than those associated with flooding, and to search analytically for the prediction of these limiting heat fluxes it may be necessary to solve the nonlinear system of equations presented in section 2.

4. CONCLUSIONS

An analytical model has been presented to study the steady state and stability thresholds of a closed two-phase thermosyphon. Although the derived model accounts for the subcooling of the liquid film and nonlinear thermohydrodynamic interaction between the liquid film and vapor core in the thermosyphon, only a special case of this model has been investigated corresponding to the saturated liquid film. A linear stability analysis predicts the loss of stability of the system as the heat flux is increased to the evaporator and leading to an instability when the liquid pool dries out and when the flooding condition is established in the thermosyphon. The steady-state distribution of the input heat flux parameter, Q_i^*, as a function of the film thickness and independent parameters of the system (N_L, Ca, l^*, h^*, ρ^* and μ^*) shows the existence of a maximum heat flux for large fillings, whereas for small fillings no such maximum is predicted. Based on a comparison of the model predictions with the experimental data, it is shown that the predicted maximum heat flux can be associated with the entrainment or flooding heat flux limit. A nonlinear analysis of the general model presented in the paper has not been performed to examine the system of equations which may yield an oscillatory behavior such as the one experimentally observed and labelled as the oscillation limit. Clearly, the conditions affecting the limiting operation of a thermosyphon are very complex, and many more careful experiments are needed to understand the limiting system operation under the increasing and decreasing heat fluxes.

REFERENCES

1. H. Cohen and F. J. Bayley, Heat transfer problems of liquid cooled gas-turbine blades, *Proc. Inst. mech. Engrs* **169**, 1063–1074 (1955).
2. B. S. Larkin, An experimental study of the two-phase thermosyphon tube, *Trans. Can. Soc. mech. Engrs* **14**, No. B-6 (1971).
3. Y. Lee and U. Mital, A two-phase closed thermosyphon, *Int. J. Heat Mass Transfer* **15**, 1695–1707 (1972).
4. H. Kusuda and H. Imura, Boiling heat transfer in an open thermosyphon, *Bull. Japan. Soc. mech. Engrs* **16**, 1723–1740 (1973).
5. R. K. Sakhuja, Flooding constraint in wickless heat pipes, ASME 73-WA/HT-7 (1973).
6. F. E. Andros and L. W. Florschuetz, The two-phase closed thermosyphon: an experimental study with flow visualization, *Two-phase Transport and Reactor Safety*, Vol. IV, pp. 1231–1267. Hemisphere, New York (1978).
7. M. K. Bezrodnyi, The upper limit of maximum heat transfer capacity of evaporative thermosyphons, *Teploenérgetika* **25**, 63–66 (1978).
8. M. K. Bezrodnyi, S. N. Faynzilberg and Ye. A. Kondrusik, Investigation of the maximum heat transfer in annular two-phase thermosyphons, *Heat Transfer–Soviet Res.* **12**, 119–123 (1980).

9. M. K. Bezrodnyi and S. S. Volkov, Study of hydrodynamic characteristics of two-phase flow in closed thermosyphons, *Advances in Heat Pipe Technology*, pp. 115–123. Pergamon Press, Oxford (1981).
10. N. Nguyen-Chi and M. Groll, Entrainment or flooding limit in a closed two-phase thermosyphon, *Advances in Heat Pipe Technology*, pp. 147–162. Pergamon Press, Oxford (1981).
11. T. Fukano, S. J. Chen and C. L. Tien, Operating limits of the closed two-phase thermosyphon, *Proc. ASME/JSME Thermal Engng Conf.*, Vol. 1, pp. 95–101 (1983).
12. G. B. Wallis, *One Dimensional Two-Phase Flow*. McGraw-Hill (1969).
13. D. Bharathan, G. B. Wallis and H. J. Richter, Air–water counter-current annular flow, EPRI Report NP-1165 (1979).

CARACTERISTIQUES STATIONNAIRES ET FRONTIERES DE STABILITE D'UN THERMOSIPHON DIPHASIQUE ET FERME

Résumé—Une étude analytique est présentée dans le but de déterminer les caractéristiques stationnaires et les frontières de stabilité d'un thermosiphon diphasique et fermé. Le modèle analytique est basé sur une description du système par paramètres localisés qui inclut la thermohydraulique du coeur de vapeur, du film liquide et de la masse liquide de l'évaporateur. Les solutions stationnaires et l'analyse de stabilité linéaire des équations révèlent l'existence de deux limites opératoires: l'une associée à l'engorgement et l'autre à l'assèchement du liquide dans l'évaporateur. Une étude paramétrique est conduite pour déterminer les effets de la géométrie du caloduc, du remplissage de liquide et des caractéristiques du fluide sur les limites opératoires. On conduit aussi la comparaison des flux thermiques limites à l'engorgement et à l'assèchement obtenus par le calcul avec les données expérimentales.

GESCHLOSSENER ZWEI-PHASEN-THERMOSYPHON—DAS VERHALTEN IM STATIONÄREN ZUSTAND UND DIE STABILITÄTSGRENZE

Zusammenfassung—Das Verhalten im stationären Zustand und die Stabilitätsgrenze eines Zwei-Phasen-Thermosyphons wurden analytisch untersucht. Das analytische Modell baut auf einer Systembeschreibung mit konzentrierten Parametern auf. Es enthält das thermohydraulische Verhalten des Dampfkerns, des Flüssigkeitsfilms und des Flüssigkeitssumpfes im Verdampfer. Die Lösungen für den stationären Zustand und die lineare Stabilitätsuntersuchung der wesentlichen Gleichungen zeigen das Vorhandensein zweier Arbeitsgrenzen: Die eine ist mit dem Überfluten, die andere mit dem Austrocknen der Flüssigkeit im Verdampfer verbunden. Zusätzlich wurde eine Parameterstudie durchgeführt, um den Einfluß der Wärmerohrgeometrie, der Füllmenge und der Fluideigenschaften auf die Arbeitsgrenzen zu bestimmen. Außerdem wurden die berechneten Grenz-Wärmestromdichten für Überflutung und Austrocknen mit Versuchsdaten verglichen.

СТАЦИОНАРНЫЕ ХАРАКТЕРИСТИКИ И ПОРОГИ УСТОЙЧИВОСТИ ЗАМКНУТОГО ДВУХФАЗНОГО ТЕРМОСИФОНА

Аннотация—В работе представлено аналитическое исследование стационарных характеристик и порогов устойчивости замкнутого двухфазного термосифона. Аналитическая модель основана на описании системю с помощью сосредоточенного параметра, которое учитывает термогидравли-